Density dependence of the symmetry free energy of hot nuclei

S. K. Samaddar,[1] J. N. De,[1] X. Viñas,[2] and M. Centelles[2]
[1]*Saha Institute of Nuclear Physics, 1/AF Bidhannagar, Kolkata 700064, India*
[2]*Departament d'Estructura i Constituents de la Matèria and Institut de Ciències del Cosmos, Facultat de Física, Universitat de Barcelona, Diagonal 647, 08028 Barcelona, Spain*
(Received 15 April 2008; revised manuscript received 11 August 2008; published 19 September 2008)

The density and excitation energy dependence of symmetry energy and symmetry free energy for finite nuclei are calculated microscopically in a microcanonical framework, taking into account thermal and expansion effects. A finite-range momentum and density-dependent two-body effective interaction is employed for this purpose. The role of mass, isospin, and equation of state (EOS) on these quantities is also investigated; our calculated results are in consonance with the available experimental data.

DOI: 10.1103/PhysRevC.78.034607 PACS number(s): 25.70.Pq, 25.70.Gh, 25.70.Mn, 21.30.Fe

I. INTRODUCTION

The symmetry energy is a measure of the energy involved in converting the excess neutrons to protons in asymmetric nuclear matter. A kinetic contribution to it comes from the associated shift of the neutron (n) and proton (p) Fermi energies; another contribution comes from the difference between the (n-p) interaction and that between like pairs (n-n or p-p). Traditionally, the symmetry energy per nucleon or the symmetry energy coefficient C_E of infinite nuclear matter has been determined from fits of experimental binding energies with various versions of the liquid drop formula [1]. But it refers only to the saturation density and at a temperature $T = 0$. Its value is usually taken to be between 30 and 35 MeV.

Understanding the details of the structure, mass, and the cooling of neutron stars [2] or simulating the dynamics of supernovae collapse [3] entails a knowledge of the density and temperature dependence of the symmetry energy. The abundance of relatively heavier elements in explosive nucleosynthesis or even the existence of exotic neutron or proton-rich nuclei produced in collisions of radioactive nuclei have a direct lineage to this knowledge. The neutron skin thickness of heavier nuclei has also been found to be intimately correlated to the density derivative of the symmetry energy [4–6] as it reflects the pressure difference on the neutrons and protons.

Collisions between nuclei at relativistic energies offer the best hope of studying properties related to isospin asymmetry (symmetry energy, symmetry free energy, etc.) of nuclear matter at supranormal densities. Inference can be made there from comparison of theoretical prediction with experimental data on symmetry energy-sensitive observables like differential flow of neutrons and protons or from the multiplicity ratio of π^-/π^+, K^0/K^+, etc. [7,8], but no firm conclusions can yet be made because the experimental isospin-sensitive signals cannot be considered very definitive [9]. At subnormal densities, studies on nuclear multifragmentation offer a unique tool to determine the characteristics of the nuclear symmetry energy or symmetry free energy as a function of density and excitation energy. In intermediate energy heavy-ion collisions, a hot dilute nuclear system is formed that expands to reach the equilibrium state and ultimately fragments into many pieces. The produced fragments bear signatures of the properties of the hot expanded system prior to fragmentation. These include the excitation energy dependence of temperature (caloric curve) and density as well as the symmetry energy and symmetry free energy at subnormal densities produced at different excitations. Data related to isotopic distributions [10], isospin diffusion [11–13], and isoscaling [14,15] have recently been analyzed and estimates of symmetry coefficients at different densities and excitations have been obtained. These estimates give somewhat different predictions and are also not fully conclusive.

There have been numerous studies on the symmetry energy of nuclear matter based on the different many-body theories using various nucleon-nucleon interactions or interaction Lagrangians [7]. These studies provide very useful tools for understanding the properties of hot and dense nuclear matter. It has been noticed that the calculated density dependence of the symmetry energy coefficient differs appreciably depending on the choice of the theoretical models and interactions. For the symmetry free energy of infinite nuclear matter, there are recent investigations done in the mean-field framework [16]. In Refs. [17,18], the symmetry energy and symmetry entropy of very dilute nuclear matter have been calculated exploiting virial expansion techniques where clusterization of light fragments is taken into account.

For finite systems, however, there are fewer available calculations for the symmetry energy or the symmetry free energy and for their dependence on density and energy. In Ref. [19], symmetry free energy coefficients of fragments produced in nuclear multifragmentation have been calculated from the variance of the isotopic distributions obtained in a statistical multifragmentation model. The present authors have performed a calculation [20] of the symmetry energy coefficient of finite nuclei based on the finite-temperature Thomas-Fermi (FTTF) formulation. This calculation was done microscopically in a microcanonical framework using a finite range, momentum, and density-dependent effective interaction [21]. The calculated symmetry energy coefficients at different excitations and densities were compared with the available scant experimental data. There is an ongoing discussion regarding whether the experimental data for the symmetry coefficients should be connected to the symmetry

 ©2008 The American Physical Society

energy or to the symmetry free energy [22]. We take the viewpoint that they refer to the symmetry free energy, in accord with recent studies [18,19]. In the present work we calculate the symmetry free energy coefficient for a number of nuclei in the FTTF formulation. The calculation of the symmetry energy coefficient in Ref. [20] was done in the local density approximation (LDA). Calculations with some improvement over the LDA are reported in the present article. In addition, the dependence of the symmetry coefficients on the mass and isospin content of the nucleus as well as on the underlying equation of state (EOS) are considered.

The organization of the article is as follows. In Sec. II, outlines of the model used in the calculation are presented. Section III contains the results and discussions. Concluding remarks are given in Sec. IV.

II. THEORETICAL FRAMEWORK

The methodology employed to calculate the symmetry energy and symmetry free energy coefficients as a function of excitation energy or density is outlined in the following.

A. Modeling the hot nucleus

When two nuclei collide at intermediate energy a hot nuclear system of neutrons and protons is formed, which is assumed to be in thermodynamic equilibrium and can be described by a temperature T. The density profile of this hot system is generated in the FTTF approximation with a chosen two-body effective interaction. The details of the employed FTTF procedure are already documented in Ref. [23] and we do not present them here.

For an expanding system pursuing the equilibrium configuration (as described later), the surface diffuseness is likely to play an important role [24]; thus, a zero-range force like the Skyrme interaction widely used to explore nuclear ground-state properties may not be very suitable for generating such a density profile. It is further noted that a constrained expanded system in the FTTF approach may lead to numerical instabilities [25,26] and the gradient (surface) terms in the energy-density functional were replaced with a suitable Yukawa interaction. We have therefore chosen a modified Seyler-Blanchard (SBM) effective interaction for the FTTF calculations. This interaction is of finite range with momentum and density dependence and is given by [21]

$$v_{\rm eff}(\mathbf{r}_1,\mathbf{r}_2,p,\rho) = -C_{l,u}\left[1-\frac{p^2}{b^2}-d^2\{\rho(\mathbf{r}_1)+\rho(\mathbf{r}_2)\}^n\right] \times \frac{\exp(-r/a)}{(r/a)}. \quad (1)$$

An effective isospin dependence in the interaction is brought through the different strength parameters C_l for like-pair (n-n, p-p) and C_u for unlike pair (n-p). The relative separations of the nucleons in configuration and momentum space are given by $r = |\mathbf{r_1} - \mathbf{r_2}|$ and $p = |\mathbf{p_1} - \mathbf{p_2}|$. The densities at the sites of the two interacting nucleons are given by $\rho(\mathbf{r_1})$ and $\rho(\mathbf{r_2})$. The parameter a corresponds to the range of the interaction, b and d determine its momentum and density dependence; the density exponent n controls the stiffness of the nuclear EOS. This interaction reproduces quite well the ground-state binding energies, root-mean-square charge radii, and isoscalar giant monopole resonance energies for a host of even-even nuclei. With a density exponent $n = 1/6$, the incompressibility of symmetric nuclear matter K_∞ is 238 MeV. A stiff EOS with $K_\infty = 380$ MeV can be simulated with $n = 4/3$.

In the FTTF approach, the nucleon density profile at temperature T has the form

$$\rho_\tau(r) = A_T^*(r) J_{1/2}[\eta_\tau(r)], \quad (2)$$

where

$$A_T^*(r) = \frac{4\pi}{h^3}[2m_{\tau,k}(r)T]^{3/2}, \quad (3)$$

and $J_K(\eta_\tau)$ is the Fermi integral

$$J_K(\eta_\tau) = \int_0^\infty \frac{x^K}{1+\exp(x-\eta_\tau)}dx, \quad (4)$$

with the fugacity η_τ given as

$$\eta_\tau(r) = [\mu_\tau - \mathcal{V}_\tau(r)]/T. \quad (5)$$

In Eqs. (2)–(5), τ is the isospin index, $m_{\tau,k}$ the effective k mass of the nucleon coming from the momentum dependence of the interaction, μ_τ the chemical potentials, and $\mathcal{V}_\tau(r)$ the effective single-particle (SP) potential (Coulomb included).

When $\eta \ll 0$, the system is very dilute with $\mathcal{V} \sim 0$ and then $\rho \sim e^{\mu/T}$, a constant. At large distances, the particle density therefore does not vanish. The pressure at the surface is then nonzero, making the system thermodynamically unstable; the density then depends on the size of the box in which the FTTF calculations are performed. This problem is overcome in the subtraction procedure [27,28], where the hot nucleus, assumed to be a thermalized system in equilibrium with a surrounding gas representing evaporated nucleons, is separated from the embedding environment. The method is based on the existence of two solutions to the FTTF equations, one corresponding to the liquid phase with the surrounding gas (lg) and other corresponding to the gas (g) phase. The density profile of the hot nucleus in thermodynamic equilibrium is given by $\rho_\tau = \rho_{\tau,lg} - \rho_{\tau,g}$. It is independent of the box size in which calculations are done. It also goes to zero at large distances, implying a vanishing surface pressure. We call this the base density (it is also sometimes called the liquid profile). The conservation of the nucleon number of each species N_τ of the hot nucleus gives

$$\int [\rho_{\tau,lg}(r) - \rho_{\tau,g}(r)]d\mathbf{r} = N_\tau. \quad (6)$$

The energy E of the required nucleus is given by

$$E = E_{lg} - E_g, \quad (7)$$

where E_{lg} and E_g are the total energies of the liquid-gas system and of the gas alone.

The total entropy in the Landau quasiparticle approximation is

$$S = -\sum_{\tau} \int g_\tau(\varepsilon_\tau, T)[f_\tau \ln f_\tau + (1 - f_\tau)\ln(1 - f_\tau)]d\varepsilon_\tau, \tag{8}$$

where f_τ is the single-particle occupancy function

$$f_\tau(\varepsilon_\tau, \mu_\tau, T) = \{1 + \exp[(\varepsilon_\tau - \mu_\tau)/T]\}^{-1}, \tag{9}$$

and g_τ is the subtracted single-particle level density. Once the energy and entropy are known, the free energy is calculated from $F = E - TS$.

In the above, the description of the hot nucleus is grand canonical obtained from the minimization of the grand potential (the temperature is a constant). In experimental conditions, however, when two nuclei collide, the hot system is formed in isolation, its total excitation energy remains a constant. The system might be compressed initially, resulting in a collective flow in the decompression stage but we ignore it in the present work. The system is microcanonical; to attain equilibrium, it expands in quest of maximum entropy. It is, however, still possible to describe the system statistically by an effective temperature T. It has the operational advantage that it helps in defining an occupation function that can be employed in evaluating various observables like energy, entropy, and so on.

The expansion of the hot nucleus is simulated through a self-similar scaling approximation for the density,

$$\rho_\lambda(r) = \lambda^3 \rho(\lambda r), \tag{10}$$

where the scaling parameter λ is unity for the unbloated nucleus and decreases with expansion, lying in the range $0 < \lambda \leqslant 1$; $\rho_\lambda(r)$ is the scaled density and $\rho(r)$ is the base density profile generated in the subtracted FTTF framework. In addition to its simplicity, there is no *a priori* justification for this choice; however, it has been shown that with a harmonic oscillator potential, at relatively small temperatures, the scaled density profiles and those generated self-consistently in a constrained Thomas-Fermi [25] procedure are equivalent [29].

One further needs to account properly for the effect of collectivity, as the coupling of the single-particle motion with the collective degrees of freedom [30] is not included in the FTTF procedure. This coupling introduces an extra energy dependence in the nucleon effective mass (m_ω, the ω mass) in addition to the k mass. The total effective mass m^* can then be written as

$$m^* = m\frac{m_k}{m}\frac{m_\omega}{m}. \tag{11}$$

The ω mass is surface-peaked and has values generally larger [31] than the nucleon mass m. This increase brings down the excited states from higher energy to lower energy near the Fermi surface, thus increasing the many-body density of states at low excitations. The system can then accommodate comparatively more entropy at a given excitation energy. The coupling of collectivity with the nucleonic single-particle motion may thus have a significant role in getting the equilibrium maximal entropy configuration. A self-consistent evaluation of m_ω is very involved; for simplicity, we take the same phenomenological form of Refs. [32–34] for it. An in-depth presentation of our computational method of the expanded hot nucleus with inclusion of collectivity can be found in Ref. [29] and thus we do not dwell further on it here.

B. Symmetry energy

The symmetry energy $e_{\rm sym}$ of nuclear matter characterizes how the energy rises as one moves away from equal numbers of neutrons and protons. For asymmetric nuclear matter at density $\rho = \rho_n + \rho_p$ with asymmetry parameter $X = (\rho_n - \rho_p)/\rho$, the symmetry energy is defined as

$$e_{\rm sym}(\rho, T, X) = e(\rho, T, X) - e(\rho, T, X = 0), \tag{12}$$

where e is the total energy per nucleon of nuclear matter, given as

$$e(\rho) = \left[\frac{\hbar^2}{2m^*}\tau(\rho) + \mathcal{E}_I(\rho)\right]\frac{1}{\rho}. \tag{13}$$

In the above equation, the first and second terms within the square brackets are the kinetic and potential energy densities for infinite nuclear matter at a density ρ.

The symmetry energy can be written as

$$e_{\rm sym}(\rho, T, X) = C_E(\rho, T)X^2 + \mathcal{O}(X^4). \tag{14}$$

The terms beyond X^2 are negligible for values of X one encounters in nuclei. The nuclear matter symmetry energy coefficient C_E is obtained from [17]

$$C_E(\rho, T) = \frac{1}{2}\frac{\partial^2}{\partial X^2} e_{\rm sym}(\rho, T, X)|_{X=0}. \tag{15}$$

The symmetry free energy coefficient C_F can similarly be defined as

$$C_F(\rho, T) = \frac{1}{2}\frac{\partial^2}{\partial X^2} f_{\rm sym}(\rho, T, X)|_{X=0}, \tag{16}$$

where $f_{\rm sym}(\rho, T, X)$ is the symmetry free energy per nucleon defined in the same manner as in Eq. (12) with e replaced by f.

To compute the coefficients C_E and C_F in finite nuclei we adopt the following prescription. Once the neutron and proton equilibrium density profiles of a nucleus with N_0 neutrons and Z_0 protons ($A_0 = N_0 + Z_0$) at an excitation energy E^* and temperature T are known, the symmetry energy coefficient can be calculated in the LDA as [20]

$$C_E(E^*)\left(\frac{N_0 - Z_0}{A_0}\right)^2 = \frac{1}{A_0}\int \rho(r)C_E(\rho(r), T)X^2(r)d\mathbf{r}. \tag{17}$$

Here, $C_E(\rho(r), T)$ is the symmetry energy coefficient at temperature T of infinite nuclear matter at a density equal to the local density $\rho(r)$ of the nucleus and $X(r) = [\rho_n(r) - \rho_p(r)]/\rho(r)$ is the local isospin asymmetry. One can obtain analogously the symmetry free energy coefficient $C_F(E^*)$ of a finite nucleus.

In the LDA, the particles at each point in space feel the potential as if it were locally a constant. The neutron and proton potentials in the configuration space are calculated at a temperature T for infinite matter at a value of the local

density $\rho(r)$ to evaluate $C_E[\rho(r), T]$ or $C_F[\rho(r), T]$. In a finite nucleus, these potentials at any point should also contain information on the densities at nearby points, which in the extended Thomas-Fermi (ETF) [35] method is taken into account by recasting the kinetic energy density as a functional of not only the local density but also its derivatives. The correction to the energy density at a temperature T, up to second order in $\hbar$ is [35,36]

$$\mathcal{E}_2(\rho) = \mathcal{F}_2(\rho) + T\sigma_2(\rho), \tag{18}$$

where $\mathcal{F}_2(\rho)$ and $\sigma_2(\rho)$ are the corrections to the free energy density and entropy density, respectively. They are given as

$$\mathcal{F}_2(\rho) = \frac{\hbar^2}{2m}\left\{\zeta(\eta) f\frac{(\nabla\rho)^2}{\rho} + \left[\frac{9}{4}\zeta(\eta) - \frac{7}{48}\right]\rho\frac{(\nabla f)^2}{f} + \frac{1}{6}(\rho\Delta f - f\Delta\rho) + \left[3\zeta(\eta) - \frac{5}{12}\right]\nabla\rho\cdot\nabla f\right\}, \tag{19}$$

and

$$\sigma_2(\rho) = -\frac{\hbar^2}{2m}\frac{\nu(\eta)}{T}\left\{f\frac{(\nabla\rho)^2}{\rho} + \frac{9}{4}\rho\frac{(\nabla f)^2}{f} + 3\nabla\rho\cdot\nabla f\right\}. \tag{20}$$

In the above two equations, ρ refers to the local density $\rho(r)$ and $f = m/m^*(r)$ is a functional of ρ. The quantity $\zeta(\eta)$, to a good approximation, is

$$\zeta(\eta) \simeq \tfrac{1}{36}[1 + 2/\sqrt{1+e^{\eta}}], \tag{21}$$

and

$$\nu(\eta) = -3\frac{J_{1/2}(\eta)}{J_{-1/2}(\eta)}\frac{d\zeta}{d\eta}. \tag{22}$$

The corrections $\mathcal{E}_2(\rho)$ and $\mathcal{F}_2(\rho)$ are added to the local energy and free energy densities perturbatively, in the spirit of variational Wigner-Kirkwood theory [37], to calculate the improved symmetry energy and symmetry free energy coefficients.

C. Isotopic scaling and symmetry free energy

It has been observed by various experimental groups [38–42] that the logarithm of the ratio R defined as

$$R = Y_2(N, Z)/Y_1(N, Z), \tag{23}$$

where Y_1 and Y_2 are the yields of a particular fragment with N neutrons and Z protons from two different fragmenting sources differing in the neutron-proton ratio at the same temperature follow a relation of the type

$$\ln R = K + (\alpha N + \beta Z). \tag{24}$$

This observation is known as isoscaling; the coefficients α and β are the parameters characterizing the isoscaling behavior and K is the normalization factor.

The parameter α has been related to the symmetry coefficient C through the relation

$$\alpha = \frac{4}{T}C\left[\left(\frac{Z_0}{A_0}\right)_2^2 - \left(\frac{Z_0}{A_0}\right)_1^2\right], \tag{25}$$

where the suffixes 1 and 2 correspond to the two fragmenting systems. The quantities $(Z_0, A_0)_i$ denote the values in the fragmenting system from whose disassembly the fragment (Z, A) is produced. Various authors have derived Eq. (25) under different approximations [10,12,42] and the coefficient C has commonly been related to the symmetry energy coefficient C_E. In this interpretation, the isospin dependence of entropy has been neglected, which may be a fair approximation at around normal density but may not be so for low densities as encountered in the tail region of the density profile of a nucleus at a relatively high temperature. In some recent literature [18,19], the need to include the asymmetry dependence of entropy has been stressed and the symmetry coefficient in Eq. (25) has been interpreted as that pertaining to the symmetry free energy. Furthermore, whether the symmetry coefficient refers to the fragmenting source or to the primary fragments at freeze-out is not fully settled. In Ref. [42], it is interpreted as the symmetry coefficient of the primary fragments. In Ref. [10], the basic interpretation is the same, but the properties of the fragments are conjectured to be modified due to "in-medium" effects because of presence of other neighboring fragments in the freeze-out volume. In the sequential Weisskopf model in the grand canonical limit [12] as applied for an expanding emitting nucleus, the symmetry coefficient is linked to that of the fragmenting source. In our present communication, we take the symmetry coefficient to be the symmetry free energy of the expanded mononuclear system in its most probable configuration at a fixed excitation energy E^*.

III. RESULTS AND DISCUSSIONS

A. Infinite nuclear matter

The SBM interaction, as mentioned earlier, reproduces well the bulk properties of nuclei. For symmetric nuclear matter as well as for neutron matter, the EOS obtained [43,44] with this interaction also compares very favorably with those calculated microscopically with realistic interactions in a variational approach [45,46]. In Fig. 1, we display the symmetry energy

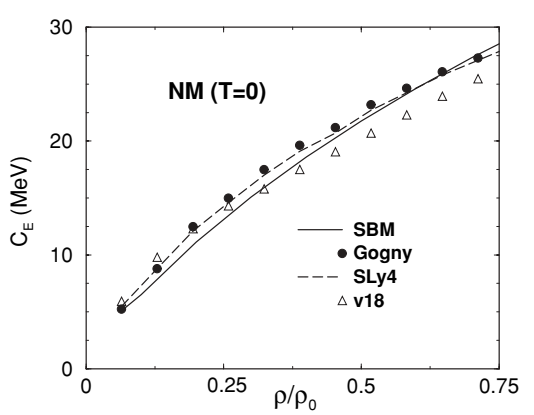

FIG. 1. The symmetry energy coefficient C_E for nuclear matter at $T = 0$ as a function of density with different interactions. The full line refers to calculations with SBM interaction; the other results are taken from Ref. [47].

coefficient of nuclear matter (at $T = 0$) as a function of density. Because our focus of interest is in the subnuclear density region, the results are presented up to $\rho \simeq 0.75\rho_0$ where ρ_0 is the saturation density taken as 0.154 fm^{-3}, its value for the SBM interaction. The calculated results are seen to be well within the range obtained in microscopic calculations [47] with different bare (Argonne v18) and effective (SLy4 and Gogny) interactions.

Up to the saturation density the symmetry energy coefficient calculated with the SBM interaction can be very well represented by

$$C_E(\rho) \simeq C_E(\rho_0)\left(\frac{\rho}{\rho_0}\right)^{\gamma}, \tag{26}$$

with $C_E(\rho_0) = 34.0$ MeV and $\gamma = 0.65$. Though the experimentally extracted value of the exponent γ is still fraught with some uncertainties, significant constraints on it have been determined from different observables in recent years. Comparison of results from the transport model with recent experimental data on isospin diffusion constrain the value of γ to around 0.69–1.05 at subnuclear densities [7]. The neutron and proton transverse emission ratio measurements [48] present some new constraints on γ somewhat larger than 0.5, whereas measurements from isotopic distributions [15] provide a value of γ close to 0.69. Consideration of the giant dipole resonance properties of ^{208}Pb puts a constraint $23.3 < C_E(\rho \sim 0.1\ \text{fm}^{-3}) < 24.9$ MeV [49], which implies a value of $\gamma \sim 0.55$.

In Fig. 2, the symmetry coefficients C_E and C_F as a function of density of nuclear matter are shown at $T = 10$ MeV in the upper panel. The difference between C_E [Eq. (27)] and C_F [Eq. (16)] is amplified with decrease in density, in consonance with that obtained in Ref. [16]. This is understandable from entropy considerations. Our calculations have been done in the mean-field model, inclusion of cluster formation at low densities would increase the values of these coefficients somewhat [17]. We find that the equilibrium density (i.e., the state at zero pressure) of nuclear matter falls off linearly with excitation energy and may be very well represented by $\rho = \rho_0(1 - 0.04E^*/A)$, with E^* expressed in MeV. The symmetry coefficients C_E and C_F for different excitations at equilibrium densities calculated using Eqs. (15) and (16) are shown in the lower panel of the figure. The dependence of these coefficients with excitation is found to be nearly linear and may be well represented as $C_E(E^*/A) \simeq C_E(0)(1 - 0.024E^*/A)$ and $C_F(E^*/A) \simeq C_F(0)(1 - 0.028E^*/A)$. We have studied the role on C_E and C_F of using a soft EOS ($n = 1/6$, $K_\infty = 238$ MeV) and a hard EOS ($n = 4/3$, $K_\infty = 380$ MeV). The effect of the EOS on both the coefficients in infinite nuclear matter is found to be small except at very low densities.

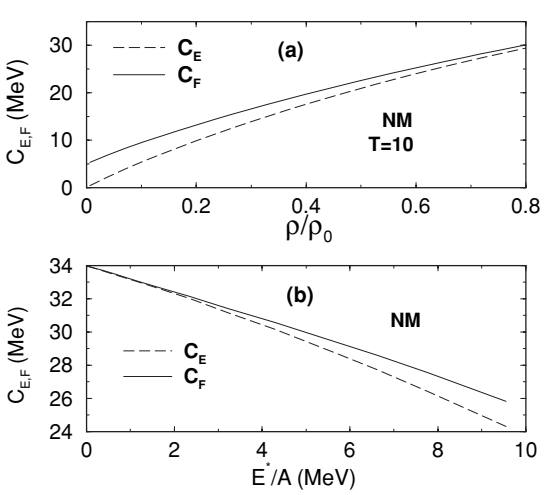

FIG. 2. The symmetry coefficients C_E and C_F for nuclear matter calculated with the SBM interaction (a) shown as a function of density at $T = 10$ MeV and (b) as a function of excitation energy.

B. Finite nuclei

We have calculated the symmetry coefficients for a number of nuclei to study their mass and asymmetry [$X_0 = (N_0 - Z_0)/A_0$] dependence as a function of density and excitation energy. For the mass dependence, we have chosen ^{197}Au and ^{40}S, both having practically the same X_0. For the isospin dependence, we have considered the isobar pair ^{150}Sm and ^{150}Cs. The relevant experimental data on the symmetry coefficients are very few; they are available mostly in the mass region $A_0 \sim$ 100–120 [15,50]. We have therefore studied the nucleus ^{110}Sn to have a comparison of the calculated results with the experimental data. The model is tested further in a wider perspective; we calculate the evolution with excitation of temperature (caloric curve) and density of this nucleus as experimental data [51,52] are available around this mass number.

1. Grand canonical approach

In Fig. 3, the caloric curve, the central density ρ_c in units of the ground-state central density $\rho_{c,0}$ and the symmetry

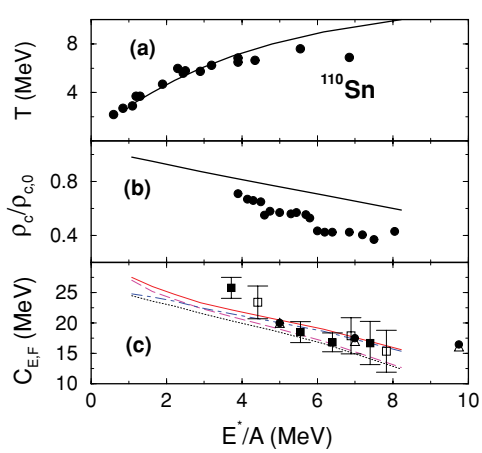

FIG. 3. (Color online) The equilibrium temperature (a), the equilibrium central density (b), and the symmetry coefficients (c) as a function of excitation energy for ^{110}Sn. The calculations are performed with the base density (without self-similar expansion). In the bottom panel, the dotted black line and the dash-dot blue line are the symmetry coefficients C_E and C_F, respectively, calculated in LDA. The dashed magenta line and the solid red line refer to C_E and C_F with inclusion of second-order corrections. For the experimental data points, see the text.

coefficients C_E and C_F for the nucleus ^{110}Sn are displayed as a function of excitation energy E^*/A in panels (a), (b), and (c), respectively. These calculations have been performed with the base density profile generated in the grand canonical framework where all the excitation energy has been locked in the thermal mode, i.e., there is no expansion energy. The experimental data for the caloric curve and densities correspond to medium-heavy nuclei ($100 < A_0 < 140$). They have been taken from Ref. [51] for the caloric curve and from Ref. [52] for the densities. We have also included in the figure the available experimental data for the symmetry coefficients; the open triangles and the filled circles are from Ref. [15] and the open and filled squares are from Ref. [50]. As discussed earlier, we interpret these data as pertaining to the symmetry free energy coefficient. The data from Ref. [15] correspond to collisions between mass-symmetric nuclei with total mass $A_0 = 116$. The source size was taken there to be somewhat less, $A_0 \simeq 100$, because of the reduction due to pre-equilibrium emission. The data in Ref. [50] were extracted for collisions of ^{12}C on ^{112,124}Sn. The symmetry coefficients there are given as a function of temperature. We have expressed them as a function of excitation energy using the Fermi-gas expression $E^* = aT^2$ with an effective level density parameter $a = A/10$.

The present calculations are done for the fragmenting source ^{110}Sn to give an orientation on the excitation energy dependence of the symmetry coefficients. As reported later, the symmetry coefficients are found to be weakly dependent on the mass of the fragmenting system but somewhat sensitive to its N_0/Z_0 ratio. The dotted black line and dot-dash blue line of Fig. 3 correspond to calculations in the LDA for C_E and C_F, respectively. The corresponding calculations with second-order corrections incorporated are represented by the magenta dash line and the full red line. The calculated caloric curve matches very well with the experimental data except at high excitations. The calculated densities are, however, overestimated. Correlation of the symmetry coefficients with the density is displayed in Fig. 4. The notations used for the different lines are the same as in the bottom panel of Fig. 3. In Fig. 3(c), it is seen that the calculated symmetry free energy coefficients follow the experimental trend rather well, but in Fig. 4 the mismatch between theory and experiment [15] becomes very apparent, indicating the limitations of the grand canonical approach.

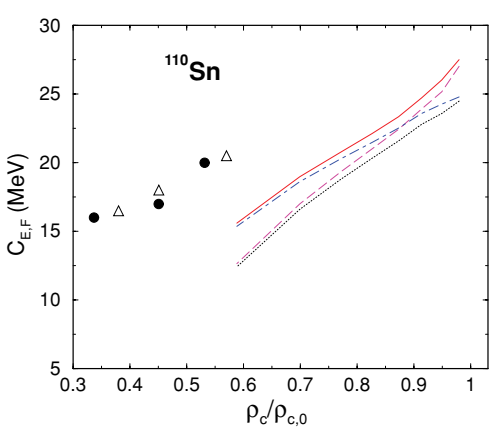

FIG. 4. (Color online) Correlation of the symmetry coefficients with density for the system ^{110}Sn. The calculations refer to those with the base density. The experimental points are taken from Ref. [15]. The notations for the calculated results are the same as described in the caption to Fig. 3(c).

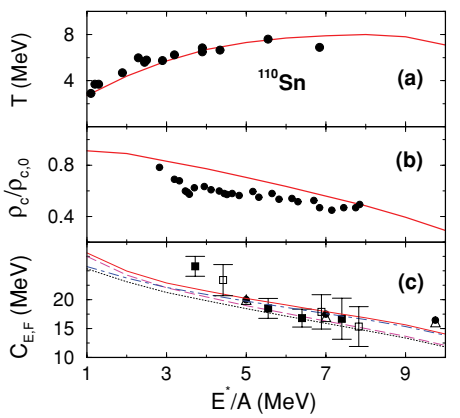

FIG. 5. (Color online) Same as described in the caption to Fig. 3, but the calculations are done with the microcanonical equilibrium density.

2. *Microcanonical approach*

The fact is that the hot nuclear system formed in energetic nuclear collisions is an isolated system and the limitations of the grand canonical approach exposed in Fig. 4 motivate one to describe the evolution of the system in microcanonical thermodynamics. In this framework, the system expands in search of the maximal entropy configuration. In panels (a) and (b) of Fig. 5, the caloric curve and the evolution of the density with excitation energy calculated in the microcanonical approach are displayed for the system ^{110}Sn. The comparison of the observables with the experimental data is now improved, showing the importance of the proper treatment of the expansion phase for the equilibrium configuration. The bottom panel displays the symmetry coefficients C_E and C_F in the LDA and also with the inclusion of second-order corrections. The different lines have the same meaning as in the bottom panel of Fig. 3. With increase in excitation, the importance of the second-order corrections is found to decrease; this is attributed to the slower fall of the density for nuclei bloated with excitation. At higher excitations, the system becomes more expanded and dilute and a possible enhancement of the symmetry coefficients with respect to the present calculation may come from clustering at the surface [17,18].

The correlation of the symmetry coefficients with density is displayed in Fig. 6 for the same system ^{110}Sn. The notations used for the calculated results are the same as described in the caption to Fig. 4. Allowing for the uncertainties in the experimental extraction of the density and of the symmetry coefficients, it is found that the calculated correlation follows the experimental trend well. A noticeable improvement of the results over those depicted in Fig. 4 is observed.

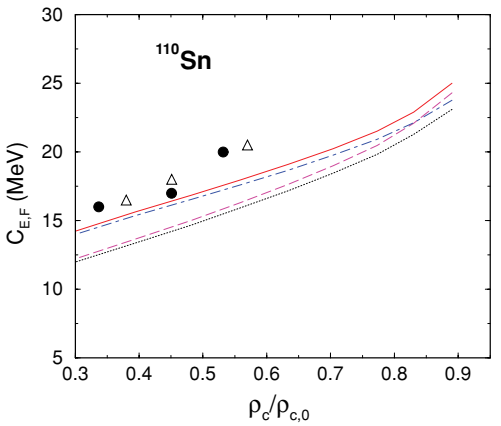

FIG. 6. (Color online) Same as described in the caption to Fig. 4 but with the microcanonical equilibrium density.

The dependence of the symmetry coefficients C_E and C_F for finite nuclei on the EOS of the underlying nuclear interaction is displayed in Fig. 7 at different excitations. We have chosen ^{110}Sn as the representative system. All the calculations presented in this figure and in Fig. 8 are done with the inclusion of the second-order corrections. At the same excitation, both C_E and C_F are larger for the stiffer EOS. This is understood from the fact that at the same excitation, the equilibrium configuration is more compact for the stiffer EOS [29]. As a whole, the symmetry coefficients are found to be not too sensitive to the choice of the EOS we have made.

The excitation energy dependence of the symmetry free energy coefficient C_F for all the five nuclei studied is displayed in panel (a) of Fig. 8. The lines from top to bottom correspond to the systems ^{110}Sn,^{197}Au, ^{150}Sm,^{150}Cs, and ^{40}S, respectively. The mass and asymmetry dependence of the symmetry coefficient can be easily inferred from the figure. The comparison of the results for the systems ^{197}Au and ^{40}S (having practically the same asymmetry) indicates the lowering of the symmetry coefficients with decreasing mass. The lighter nucleus has a lesser value of C_F because of the predominance of the surface effects. Similarly, the isospin or asymmetry dependence can be inferred from the comparison of results of the isobar pair ^{150}Sm and ^{150}Cs. The lower values

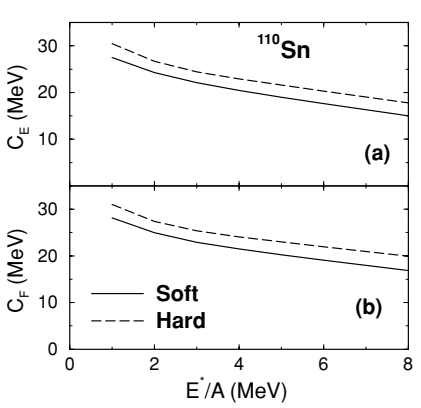

FIG. 7. The dependence of the symmetry coefficients on the underlying EOS is shown for the finite system ^{110}Sn.

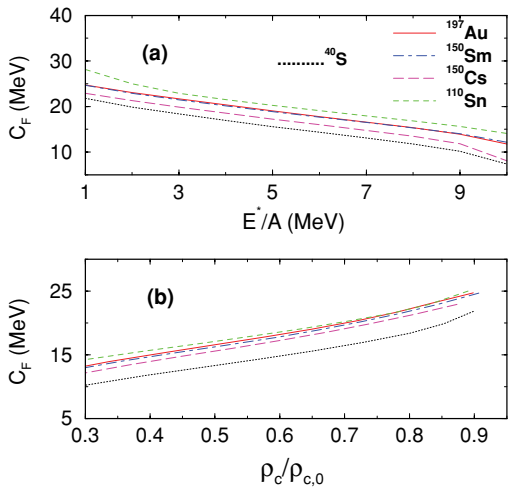

FIG. 8. (Color online) The symmetry coefficient C_F for the five nuclei studied is shown as a function of excitation energy (upper panel) and as a function of density (lower panel). From top to bottom, the lines correspond to ^{110}Sn,^{197} Au,^{150} Sm,^{150} Cs, and ^{40}S, respectively.

of the symmetry coefficient C_F for the more asymmetric nucleus ^{150}Cs can be traced to the fact that isobars with higher asymmetry have effectively softer EOS [29]. It is seen that the results for the symmetry coefficients for the pair ^{197}Au and ^{150}Sm are practically indistinguishable. This reflects an interplay of the effects due to mass and asymmetry. This is further amplified in the larger values of C_F for ^{110}Sn, which has an appreciably smaller mass than ^{197}Au but has also a very small asymmetry $X_0 = 0.09$. In panel (b) of Fig. 8, the symmetry free energy coefficients of all the nuclei studied are displayed as function of their equilibrium densities corresponding to different excitations. The variations of the density correlation of the symmetry coefficients with mass and isospin for the nuclei studied are very similar to those seen for the excitation energy in the upper panel of the figure. The results for the symmetry energy coefficient C_E exhibit nearly the same trends with excitation and density as C_F in the present figure, and therefore we do not display them.

As seen in Fig. 8, the excitation energy dependence of C_F for all the five nuclei discussed is almost linear and the results corresponding to each nucleus run nearly parallel. As in the case of nuclear matter, this dependence can be well approximated by a linear relation $C_F(E^*/A) = C_F(0)(1 - \alpha_F E^*/A)$ with $\alpha_F \simeq 0.054$ MeV^{-1}. The same holds for the symmetry energy coefficient C_E (not shown in the figure), for which we find $C_E(E^*/A) = C_E(0)(1 - \alpha_E E^*/A)$ with $\alpha_E \simeq 0.064$ MeV^{-1}. The faster falloff of the symmetry coefficients of finite nuclei with increasing excitation compared to those of nuclear matter is attributed to the comparatively lower equilibrium density of the isolated nuclei at the same excitation.

The density dependence of the symmetry free energy coefficient of the finite nuclei can be fitted with a general expression of the form

$$C_F(\rho) = \frac{\kappa_v(\rho/\rho_0)^{\gamma_1}}{1 + \kappa_s\,(\rho/\rho_0)^{\gamma_2} A^{-1/3}}\left(1 - \kappa_{\rm sym} X_0^2\right), \qquad (27)$$

where κ_v and κ_s are the volume and surface constants contributing to the symmetry coefficient. The exponents γ_1 and γ_2 depict the density dependence of the volume and surface contributions, respectively. We have included a term $\kappa_{\rm sym}\, X_0^2$, with X_0 being the asymmetry parameter of the finite nucleus. This is done to test the size of an eventual departure of the symmetry energy in finite systems from the quadratic dependence on the asymmetry parameter that is assumed in the definition of the symmetry coefficients.

A least-squares fit of Eq. (27) to the calculated values for the symmetry free energy coefficient fixing the values of κ_v (34 MeV) and $\gamma_1(0.65)$ to those of infinite nuclear matter, and considering all the five systems studied in the excitation energy range $1 \leqslant E^*/A \leqslant 10$ MeV, gives $\kappa_s = 1.46$, $\gamma_2 = 0.17$ and $\kappa_{\rm sym} = 1.55$ with a root-mean-square deviation $\simeq$6%. The significantly lower value of γ_2 compared to the volume exponent γ_1 points to a weaker surface density dependence. A free variation of all the five parameters improves the least-squares fit very little compared to the variation of three parameters mentioned above. In infinite nuclear matter, the symmetry energy and symmetry free energy are known to be well represented with a quadratic term in the asymmetry parameter X, the quartic term being negligible. In finite nuclei, the existence of surface and Coulomb effects may modify this scenario. The result $\kappa_{\rm sym} = 1.55$ found indicates, however, that the effect is relatively small for the typical values of X_0 in nuclei.

IV. CONCLUDING REMARKS

We have investigated the energy and density dependence of the symmetry energy and symmetry free energy coefficients of finite and infinite nuclear systems. The dependence of these coefficients on the EOS, mass, and isospin content of nuclei have further been explored. The calculations are done in a microscopic microcanonical framework using a momentum and density-dependent finite-range effective interaction. The density dependence of the symmetry energy coefficient of infinite nuclear matter calculated with this interaction compares very well with those obtained from other microscopic calculations.

Our main focus in the present work is to explore the density and energy dependence of the symmetry coefficients of finite nuclei. First, we have investigated the predictions of our considered model for these coefficients for infinite nuclear matter in the subnuclear density range. In the density range $0.1 < \rho/\rho_0 < 1$, the symmetry energy coefficient for nuclear matter at $T = 0$ is found to be well reproduced by $C_E(\rho) \simeq C_E(\rho_0)(\rho/\rho_0)^\gamma$ with $C_E(\rho_0) = 34.0$ MeV at the saturation density and $\gamma \simeq 0.65$, well within the experimental range of values. For finite nuclei, the calculations have been performed in the local density approximation and improved by incorporating second-order corrections in gradients of the neutron and proton densities perturbatively. The calculated symmetry free energy coefficients are found to be larger than the symmetry energy coefficients by $\sim$10% at medium excitations because of the contribution from the symmetry entropy. At low excitations, as expected, there is little difference in the values of the two coefficients. At the highest excitation (10 MeV/nucleon) that we explore, the difference is $\sim$15%. The calculated coefficients C_F compare favorably with the available experimental data.

Both for infinite nuclear matter and for finite nuclei, the symmetry coefficients vary linearly with excitation energy; however, for finite systems, the dependence is much stronger. The dependence on the EOS of the symmetry coefficients for nuclear matter is found to be rather weak. For finite systems the dependence is more noticeable and the symmetry coefficients decrease with the softness of the EOS. They are, however, not too sensitive to the EOS chosen. The coefficients C_E and C_F of finite nuclei are system dependent, an interplay of the role of mass and isospin is quite evident there. For the same asymmetry, the coefficients get smaller with smaller mass, this dependence is weak. However, for the same mass, the coefficients show a relatively stronger dependence on the isospin content of the nucleus.

The characterization of the density and excitation dependence of the symmetry term of the nuclear interaction is instrumental for the understanding of a plethora of phenomena in both nuclear physics and astrophysics. This topic currently attracts much theoretical and experimental activity. Our present calculations have been done in the mean-field framework, effects beyond mean field, like clusterization at low densities, may have perceptible effects and therefore are worth a study. The relevant experimental data are still very scarce, the continuing experimental effort in reactions with neutron-rich stable nuclei and future data from reactions with exotic isotopes in the radioactive ion beam facilities would contribute to a better understanding of these phenomena.

ACKNOWLEDGMENTS

S.K.S. and J.N.D. acknowledge the financial support from CSIR and DST, Government of India, respectively. M.C. and X.V. acknowledge financial support from Grant Nos. FIS2005-03142 from MEC (Spain) and FEDER and No. 2005SGR-00343 from Generalitat de Catalunya, as well as from the Spanish Consolider-Ingenio 2010 Programme CPAN CSD2007-00042.

[1] D. Lunney, J. M. Pearson, and C. Thibault, Rev. Mod. Phys. **75**, 1021 (2003).
[2] C. Fuchs, J. Phys. G **35**, 014049 (2008).
[3] A. W. Steiner, M. Prakash, J. M. Lattimer, and P. J. Ellis, Phys. Rep. **411**, 325 (2005).
[4] B. A. Brown, Phys. Rev. Lett. **85**, 5296 (2000).
[5] C. J. Horowitz and J. Piekarewicz, Phys. Rev. Lett. **86**, 5647 (2001).
[6] M. Baldo, C. Maieron, P. Schuck, and X. Viñas, Nucl. Phys. **A736**, 241 (2004).
[7] B. A. Li, L. W. Chen, and C. M. Ko, Phys. Rep. **464**, 113 (2008).

[8] G. Ferini, T. Gaitanos, M. Colonna, M. Di Toro, and H. H. Wolter, Phys. Rev. Lett. **97**, 202301 (2006).
[9] X. Lopez *et al*. (FOPI Collaboration), Phys. Rev. C **75**, 011901 (2007).
[10] A. S. Botvina, N. Buyukcizmeci, M. Erdogan, J. Lukasik, I. N. Mishustin, R. Ogul, and W. Trautmann, Phys. Rev. C **74**, 044609 (2006).
[11] F. Rami *et al*., Phys. Rev. Lett. **84**, 1120 (2000).
[12] M. B. Tsang *et al*., Phys. Rev. Lett. **92**, 062701 (2004).
[13] L. W. Chen, C. M. Ko, and B. A. Li, Phys. Rev. Lett. **94**, 032701 (2005).
[14] G. A. Souliotis, A. S. Botvina, D. V. Shetty, A. L. Keksis, M. Jandel, M. Veselsky, and S. J. Yennello, Phys. Rev. C **75**, 011601(R) (2007).
[15] D. V. Shetty, S. J. Yennello, and G. A. Souliotis, Phys. Rev. C **76**, 024606 (2007).
[16] J. Xu, L. W. Chen, B. A. Li, and H. R. Ma, Phys. Rev. C **75**, 014607 (2007).
[17] C. J. Horowitz and A. Schwenk, Nucl. Phys. **A776**, 55 (2006).
[18] S. Kowalski *et al*., Phys. Rev. C **75**, 014601 (2007).
[19] Ad. R. Raduta and F. Gulminelli, Phys. Rev. C **75**, 044605 (2007).
[20] S. K. Samaddar, J. N. De, X. Viñas, and M. Centelles, Phys. Rev. C **76**, 041602(R) (2007).
[21] D. Bandyopadhyay, C. Samanta, S. K. Samaddar, and J. N. De, Nucl. Phys. **A511**, 1 (1990).
[22] B. A. Li and L. W. Chen, Phys. Rev. C **74**, 034610 (2006).
[23] J. N. De, N. Rudra, S. Pal, and S. K. Samaddar, Phys. Rev. C **53**, 780 (1996).
[24] L. G. Sobotka and R. J. Charity, Phys. Rev. C **73**, 014609 (2006).
[25] U. Lombardo and G. Russo, Phys. Rev. C **36**, 841 (1987).
[26] K. T. R. Davies and S. E. Koonin, Phys. Rev. C **23**, 2042 (1981).
[27] P. Bonche, S. Levit, and D. Vautherin, Nucl. Phys. **A436**, 265 (1985).
[28] E. Suraud, Nucl. Phys. **A462**, 109 (1987).
[29] S. K. Samaddar, J. N. De, X. Viñas, and M. Centelles, Phys. Rev. C **75**, 054608 (2007).
[30] A. Bohr and B. R. Mottelson, *Nuclear Structure* (Benjamin, Reading, MA, 1975), Vol. II.
[31] R. Hasse and P. Schuck, Phys. Lett. **B179**, 313 (1986).
[32] M. Prakash, J. Wambach, and Z. Y. Ma, Phys. Lett. **B128**, 141 (1983).
[33] S. Shlomo and J. B. Natowitz, Phys. Lett. **B252**, 187 (1990).
[34] J. N. De, S. Shlomo, and S. K. Samaddar, Phys. Rev. C **57**, 1398 (1998).
[35] M. Brack, G. Guet, and H. B. Hakansson, Phys. Rep. **123**, 275 (1985).
[36] J. Bartel, M. Brack, and M. Durand, Nucl. Phys. **A445**, 263 (1985).
[37] M. Centelles, P. Schuck, and X. Viñas, Ann. Phys. (NY) **322**, 363 (2007).
[38] M. B. Tsang, W. A. Friedman, C. K. Gelbke, W. G. Lynch, G. Verde, and H. S. Xu, Phys. Rev. Lett. **86**, 5023 (2001).
[39] H. S. Xu *et al*., Phys. Rev. Lett. **85**, 716 (2000).
[40] D. V. Shetty, S. J. Yennello, E. Martin, A. Keksis, and G. A. Souliotis, Phys. Rev. C **68**, 021602(R) (2003).
[41] M. B. Tsang *et al*., Phys. Rev. C **64**, 054615 (2001).
[42] A. Ono, P. Danielewicz, W. A. Friedman, W. G. Lynch, and M. B. Tsang, Phys. Rev. C **68**, 051601(R) (2003).
[43] V. S. Uma Maheswari, D. N. Basu, J. N. De, and S. K. Samaddar, Nucl. Phys. **A615**, 516 (1997).
[44] N. Rudra and J. N. De, Nucl. Phys. **A545**, 608 (1992).
[45] B. Friedman and V. R. Pandharipande, Nucl. Phys. **A361**, 502 (1981).
[46] R. B. Wiringa, V. Fiks, and A. Fabrocini, Phys. Rev. C **38**, 1010 (1988).
[47] C. Fuchs and H. H. Wolter, Eur. Phys. J. A **30**, 5 (2006).
[48] M. A. Famiano *et al*., Phys. Rev. Lett. **97**, 052701 (2006).
[49] L. Trippa, G. Colo, and E. Vigezzi, Phys. Rev. C **77**, 061304(R) (2008).
[50] A. Le Fevre *et al*., Phys. Rev. Lett. **94**, 162701 (2005).
[51] J. Cibor *et al*., Phys. Lett. **B473**, 29 (2000).
[52] J. B. Natowitz *et al*., Phys. Rev. C **66**, 031601(R) (2002).